Reaction Chemistry & Engineering

ROYAL SOCIETY OF CHEMISTRY

PAPER

View Article Online
View Journal | View Issue

Cite this: *React. Chem. Eng.*, 2021, **6**, 1974

Dynamics of phase transitions in Na_2TiO_3 and its possible utilization as a CO_2 sorbent: a critical analysis

Maria Valeria Blanco, *[a] Paula Macarena Abdala, [b] Fabiana Gennari [cde] and Federico Cova *[a]

Received 31st March 2021,
Accepted 13th July 2021

DOI: 10.1039/d1re00125f

rsc.li/reaction-engineering

Na-Based materials are emerging as promising high-temperature CO_2 sorbents. In this work, we provide a detailed study on the synthesis of Na_2TiO_3 *via* a solid-state route using NaOH and TiO_2 as starting reactants. The CO_2 sorption properties of the synthesized Na_2TiO_3 were evaluated by thermogravimetric analysis. A subsequent comprehensive study on the complex reaction mechanism of Na_2TiO_3 at high temperatures under carbonation conditions was performed *via* real time *in situ* synchrotron X-ray diffraction analysis. *In situ* experiments performed under different conditions revealed the occurrence of thermally-driven phase transitions derived from the structural instability of the material at high temperatures. These reactions could be differentiated from carbonation processes, allowing the proposal of a reaction mechanism of the material as a CO_2 sorbent. The obtained results can explain the abnormal dynamic thermogram displayed by Na_2TiO_3 in the presence of CO_2 within a temperature range that is of interest for practical applications and serve as a basis for evaluating the feasibility of using this material in CO_2 capture schemes.

1 Introduction

Global CO_2 emissions have increased by about 90% in the last 50 years, with industrial processes and fossil fuel combustion being the two major contributors, and about 78% of the total increment having occurred in the period from 1970 to 2011.[1] Since CO_2 has been pointed out as mainly responsible for the greenhouse effect that drives global climate change, the development of strategies for mitigating its release to the atmosphere constitutes an essential prerequisite to prevent further global warming. A closer look into anthropogenic CO_2 emissions shows that approximately 40% of them are generated by power plants.[2] Hence, the design and engineering of materials and processes to capture and retain the CO_2 before its release to the atmosphere appear as a viable alternative to tackle climate change, while transitioning to more sustainable and renewable power schemes.

Solid sorbents have been proven to efficiently remove CO_2 from high-temperature industrial gas streams,[3–5] with promising results when implemented at a pilot scale in different coal-fired and cement plants.[6,7] Indeed, these materials with the ability to react with CO_2 at high temperatures have shown great potential for the separation of CO_2 in sorption enhanced reaction processes (SERPs) for hydrogen production, $CH_4 + 2H_2O \rightarrow CO_2 + 4H_2$,[8,9] where the *in situ* CO_2 removal shifts the equilibrium towards high-purity hydrogen production and increased hydrocarbon conversion. In the case of steam reforming processes (SESRs), continuous capture of CO_2 can dramatically enhance H_2 selectivity and avoid cooling processes.[10,11] Therefore, solid sorbents can be applied in either pre-combustion or post-combustion CO_2 capture schemes. Ideally, these materials should exhibit high sorption capacities, good regeneration capabilities and long-term stability, together with a low price.

Among proposed high-temperature solid CO_2 sorbents,[12] alkali and alkaline-earth oxides containing lithium, sodium, potassium, calcium and/or magnesium have shown promising properties towards CO_2 capture. When reacting with CO_2, these sorbents usually exhibit a temperature-dependent behaviour in which CO_2 is first chemisorbed,

[a] *European Synchrotron Radiation Facility, 71 Avenue des Martyrs, Grenoble, France. E-mail: federico.cova@csic.es*
[b] *Department of Mechanical and Process Engineering, ETH Zürich, Leonhardstrasse 21, CH-8092 Zurich, Switzerland*
[c] *Consejo Nacional de Investigaciones Científicas y Técnicas (CONICET), R8402AGP, S. C. de Bariloche, Río Negro, Argentina*
[d] *Centro Atómico Bariloche (CAB-CNEA), R8402AGP, S.C. de Bariloche, Río Negro, Argentina*
[e] *Universidad Nacional de Cuyo (UNCuyo), Instituto Balseiro, Av. Bustillo 9500, R8402AGP Bariloche, Río Negro, Argentina*

producing an external shell composed of either Li_2CO_3, Na_2CO_3, K_2CO_3, $CaCO_3$ or $MgCO_3$. Once the temperature is high enough to activate diffusion processes, the reaction proceeds through the bulk of the particles.

Li-Based materials, such as Li_4SiO_4, Li_2ZrO_3, Li_5AlO_4 and Li_2CuO_2, have been widely studied as CO_2 sorbents,[13] displaying high sorption capacities within the temperature range of 400–700 °C.[14–17] However, from a large-scale application perspective, low cost Na-based captors, such as Na_2TiO_3, Na_2ZrO_3, Na_2SiO_3 and Na_4SiO_4, are more attractive.[18–21] The lower cost is usually associated with the manufacture process since, as a general rule, lithium oxides are more expensive than their sodium counterparts. Given that Na-based sorbents, such as Na_2ZrO_3, can reach CO_2 sorption capacities very close to those of Li-based systems,[22,23] it is important to further explore their properties and capabilities towards CO_2 capture.

Na_2TiO_3 is a promising material for positive electrodes in Na-ion batteries[24–26] and has also been proposed as a possible CO_2 sorbent.[22,27] Interestingly, the thermogram displayed by Na_2TiO_3 when subjected to a CO_2 flow differs from those exhibited by other CO_2 sorbents. The Na_2TiO_3 thermogram shows two weight increments, which are then followed by sequential weight decrements. This experimental evidence questions the stability Na_2TiO_3 at high temperatures and its ability to trap CO_2. In addition to this, *ex situ* XRD characterization of Na_2TiO_3–CO_2 reaction products showed the formation of Na_2CO_3, Na_2O, m-$Na_4Ti_5O_{12}$, h-$Na_4Ti_5O_{12}$ and $Na_{16}Ti_{10}O_{28}$ phases.[27] The observation of these chemical species, together with the absence of TiO_2, is indicative of the partial reaction of Na_2TiO_3 with CO_2, and also suggests a complex temperature-dependent reaction mechanism. Despite the great effort to understand the reaction pathway of Na_2TiO_3–CO_2 at high temperatures,[27] the great likelihood of disproportionation of this material and its thermal instability makes standard characterization methods inaccurate. Instead, more sophisticated analysis tools that allow tracking in real time the structural changes occurring at high temperatures in the presence of CO_2 need to be employed in order to describe the reaction path and better understand the behavior of the system under operative conditions.

In this work, we present thermodynamic calculations and experimental data on the synthesis of Na_2TiO_3 *via* a solid-state route. Then, we show the benefits of using high temperature *in situ* synchrotron X-ray diffraction analysis to gain valuable insights on phase transformations that are difficult to detect by standard *ex situ* characterization techniques. *In situ* X-ray diffraction experiments revealed the occurrence of thermally driven structural changes of the material. These phase transformations could be differentiated from carbonation processes, allowing the proposal of a reaction mechanism of Na_2TiO_3 as a CO_2 sorbent. The influence of the surrounding atmosphere on the carbonation kinetics and reaction path of Na_2TiO_3 at high temperatures is discussed.

2 Experimental

2.1 Material synthesis

Sodium hydroxide (millimeter spheres of NaOH, Biopack, purity 98%) and titanium dioxide (nanopowder of TiO_2, Sigma, purity 99%, anatase ≈75 wt% and rutile ≈25 wt%) were used as starting materials. The synthesis of β-Na_2TiO_3 was performed as follows. A mixture of NaOH–TiO_2 with a 2.1 : 1 molar ratio was handled in an Ar-filled glove box and introduced into a milling chamber. The powder mixture was then milled in a planetary ball mill (Fritsch Pulverisette P6) for 15 min in an Ar atmosphere. The selected milling conditions included a ball to powder ratio of 40 : 1 and 400 rpm. After milling, the powders were pressed and heated in air at 800 °C for 5 h.

2.2 Thermodynamic calculations

The equilibrium composition of the 2NaOH–TiO_2 mixture as a function of temperature was calculated by a Gibbs free energy minimization method using HSC software (6.1 version).[28] This method determines the equilibrium products at different temperatures and pressures for a heterogeneous system based on an extensive thermochemical database which contains enthalpy, entropy and heat capacity data of chemical compounds. The reaction system was specified in terms of the number of phases, species and the initial amount of reactants. The starting reaction system was composed of 2 kmol NaOH and 1 kmol TiO_2 (75% anatase and 25% rutile) in the solid phase, and air (N_2 = 78 kmol and O_2 = 21 kmol O_2) in the gas phase. The presence of H_2O(l,g) was also contemplated. Several species were considered as possible in the solid phase: NaOH·H_2O; Na_2O; Na; NaH; Ti_3O_2; Ti_2O_3; Na_2O_2; Na_2TiO_3 (beta phase); $Na_2Ti_2O_5$; $Na_2Ti_3O_7$; $Na_2Ti_6O_{13}$. Some sodium titanates ($Na_4Ti_5O_{12}$, $Na_{16}Ti_{10}O_{28}$) previously reported were not included in the equilibrium composition calculations because of the lack of thermodynamic properties reported in the literature. Calculations were carried out in the temperature range of 0–800 °C and at 1 atm.

2.3 Characterization techniques

The structural and thermal properties of the samples were studied using X-ray powder diffraction (XRPD, Bruker D8 Advance) and simultaneous thermogravimetry and differential scanning calorimetry (TG-DSC, Linseis STA PT1600) coupled with mass spectroscopy (MS, ThermoStar Pfeiffer). *Ex situ* XRPD patterns were collected in the 2θ range of 10–80° with CuKα radiation, a voltage of 40 kV and an electric current of 40 mA. The thermal behaviour of the as-milled 2NaOH–TiO_2 mixture was measured with a heating rate of 5 °C min^{-1} from room temperature to 800 °C under a synthetic air flow (50 cm^3 min^{-1} STP). Dynamic CO_2 capture measurements were carried out with a thermogravimetric instrument (TG-HP50, TA Instruments). The as-synthesized β-Na_2TiO_3 was heated from room temperature to 800 °C at a

heating rate of 5 °C min^{-1} using a CO_2 flow rate of 50 cm^3 min^{-1} (STP).

In situ synchrotron X-ray diffraction (XRD) measurements were performed at the beamline ID31 of the European Synchrotron Radiation Facility (ESRF). For this, β-Na_2TiO_3 samples were loaded into 1 mm outer diameter quartz capillaries and then subjected to different treatments: 1) dynamic heating under a N_2 gas flow up to a final temperature of 615 °C, and then switching the gas to CO_2 and maintaining isothermal conditions for 1 h; 2) heating under a N_2 gas flow up to 770 °C and then switching the gas to CO_2 and maintaining isothermal conditions for 1 h; 3) heating under a CO_2 gas flow up to 770 °C and maintaining isothermal conditions. In all cases, the heating ramp was 5 °C min^{-1}. A sketch of the experimental setup can be found elsewhere.[29] *In situ* synchrotron X-ray diffraction data were collected using a PerkinElmer detector, at a wavelength of 0.1771 Å and with a beamsize of 0.6 mm × 0.6 mm ($V \times H$). Each frame was collected with an exposure time of 1 s. Data were processed using the pyFAI package.[30] The analysis of selected diffraction peaks representative of different crystallographic phases was performed by curve fitting with the Gaussian function, using Fityk software.[31] Rietveld refinements were performed using GSAS II software.[32]

3 Results and discussion

3.1 Synthesis and CO_2 properties of the β-Na_2TiO_3 system

3.1.1 Study of the thermal behaviour of 2NaOH–TiO_2 mixtures. The equilibrium composition of the 2NaOH–TiO_2 system was estimated based on the Gibbs energy minimization method.[28] The thermodynamic calculations displayed in Fig. 1 predict the complete consumption of TiO_2 at 0 °C, simultaneous with the formation of β-Na_2TiO_3 and H_2O(l,g) as the main reaction products.

The hydration of NaOH to NaOH·H_2O at temperatures lower than 100 °C is promoted by the H_2O formation. A progressive temperature rise to 300 °C increases the amounts of both β-Na_2TiO_3 and H_2O(g), reaching for each phase a maximum amount that remains constant for higher temperatures. From the previous interpretations, it is possible to infer that the formation of β-Na_2TiO_3 is favored thermodynamically by heating of the starting mixture in air. The expected reaction at room temperature can be expressed as:

$$2NaOH(s) + TiO_2(s) \rightarrow Na_2TiO_3(s) + H_2O(g) \quad (1)$$

where $\Delta G°$ (293 K) = −44.75 kJ mol^{-1} which is thermodynamically favorable.

From the thermodynamic calculations, it is expected that the both formation of $Na_2Ti_2O_5$ and β-Na_2TiO_3 will occur simultaneously from 0 °C; however, the $Na_2Ti_2O_5$ amount decreases to a minimum value with the temperature rising to 200 °C. A possible formation reaction is:

$$2NaOH(s) + 2TiO_2(s) \rightarrow Na_2Ti_2O_5(s) + H_2O(l,g) \quad (2)$$

As the temperature increases from 0 °C, $Na_2Ti_2O_5$ is the only titanium source to induce the production of an extra amount of β-Na_2TiO_3, consuming NaOH:

$$2NaOH(s) + Na_2Ti_2O_5(s) \rightarrow 2Na_2TiO_3(s) + H_2O(g) \quad (3)$$

Reactions (2) and (3) are also thermodynamically favorable above 0 °C and 100 °C, respectively.

Previous thermodynamic analysis determined the on-going reactions in the absence of any restrictions caused by kinetics and/or transport phenomena and can serve as a benchmark to compare with the experimental results. In order to evaluate the reactivity of the 2NaOH–TiO_2 mixture for the synthesis of β-Na_2TiO_3, TG-DSC measurements were combined with MS analysis (Fig. 2). The TG curve of the as-milled 2NaOH–TiO_2 powder shows a sharp weight loss of 13% between 50 and 200 °C, which correlates with an endothermic peak in the DSC curve. According to MS analysis, this sharp weight loss can be

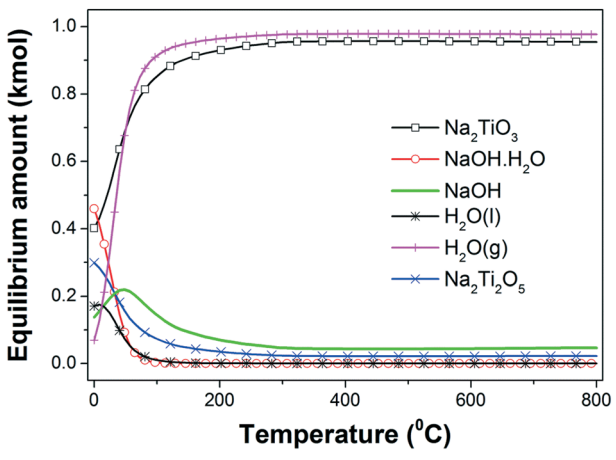

Fig. 1 Equilibrium amount (kmol) of different species in the 2NaOH–TiO_2 system as a function of temperature at 1 atm.

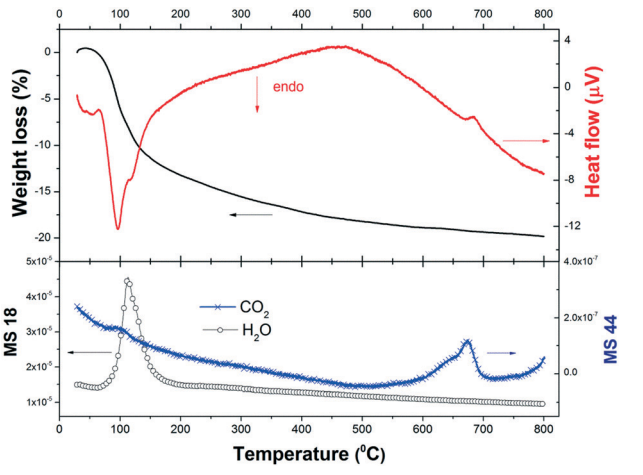

Fig. 2 Weight loss (in%), heat flow (μ V) and gas evolved (H_2O and CO_2) during heating of as-milled 2NaOH–TiO_2 in synthetic air.

ascribed mainly to water evolution due to the formation of Na_2TiO_3 (reaction (1), theoretical value of 11.3%) and also attributable to dehydration from pre-adsorbed water on NaOH. As the temperature increases up to 800 °C, the weight loss progresses to 20% and MS analysis evidences gradual water and CO_2 evolution. In the DSC curve, no melting of pure NaOH or melting of the NaOH–Na_2CO_3 eutectic mixture[33] was observed. These events are expected at about 320 °C and 282 °C, respectively. Their absence indicates that NaOH was completely consumed at temperatures lower than 282 °C and/or NaOH partially reacted with CO_2 present in the air during handling, forming Na_2CO_3.[34] CO_2 detection by MS reveals CO_2 release, evidenced by the occurrence of: a small bump at 100 °C, a gradual decline observed in the curve starting from low temperatures, and a peak between 600 and 700 °C. These events indicate that slight CO_2 adsorption occurred prior to the thermal analysis run. Additionally, an exothermic peak at 685 °C was identified and is analyzed in the following paragraph.

The *ex situ* XRPD patterns of the products obtained at different reaction temperatures are displayed in Fig. 3. As reference, the XRPD patterns of nano-TiO_2 and as-milled 2NaOH–TiO_2 powders are also included (Fig. 3a and b). After milling, the anatase and rutile phases of TiO_2 remain, while Na_2CO_3 is formed due to carbonation of NaOH during the XRD measurement in air (Fig. 3b). Thus, milling processes promote a high degree of mixing of the starting reactants, independent of the starting size of the powders. Heating at 650 °C induces the formation of α-Na_2TiO_3 (Fig. 3c) simultaneous with minor CO_2 release, as inferred from the TG curve. The most intense diffraction peaks of Na_2CO_3 are still detected, with very low intensity. At 800 °C, the main phase obtained is β-Na_2TiO_3 with $Na_{16}Ti_{10}O_{28}$ (Fig. 3d). Prolonged heating at 800 °C favors the complete crystallization of β-Na_2TiO_3 (Fig. 3e). From the XRD and TG-DSC results, it can be speculated that at 685 °C, transformation between α- and β-Na_2TiO_3 occurred during heating, in agreement with previous studies using fine rutile-TiO_2.[34]

Some correlations can be made by comparison of the TG-DSC-MS results, XRPD studies and thermodynamic calculations. TG-DSC-MS measurements show the high reactivity between NaOH and TiO_2 at temperatures lower than 200 °C, with H_2O evolution due to reaction (1) and, as a consequence, NaOH dehydration. This reaction continues as the temperature increases, showing progressive H_2O release. Similar predictions were obtained from the thermodynamic calculations up to 200 °C. However, equilibrium calculations anticipate that the reaction between NaOH and TiO_2 is almost completed at 300 °C, with the difference from experimental results being ascribed to kinetic factors. The tests show the formation of metastable α-Na_2TiO_3 at 650 °C, which transforms to β-Na_2TiO_3 upon heating. The phase transformation towards the formation of β-Na_2TiO_3 progresses during the temperature ramp up to 800 °C, however upon reaching this temperature the reaction is still incomplete and requires additional time at this temperature to achieve completion. Although α-Na_2TiO_3 and $Na_{16}Ti_{10}O_{28}$ were identified at different temperatures, their formation could not be derived from thermodynamic calculations due to the lack of thermochemical data. Heating for 5 h produces β-Na_2TiO_3 as a single phase. Therefore, nano-TiO_2 reacts with NaOH at the beginning of heating, producing water, forming α-Na_2TiO_3 as an intermediate phase and finally producing β-Na_2TiO_3 at 800 °C after prolonged heating.

3.1.2 Thermogravimetric characterization of the reaction of β-Na_2TiO_3 with CO_2. To study the CO_2 sorption behaviour of as-synthesized β-Na_2TiO_3, dynamic CO_2 measurements were performed. The results displayed in Fig. 4 show a continuous CO_2 capture up to 3.5 wt% from room temperature to 400 °C, followed by a progressive weight loss of 1.5 wt% until 600 °C. After that, a sharp CO_2 absorption peak was registered from 620 °C to 800 °C, with 8.0 wt% CO_2 captured.

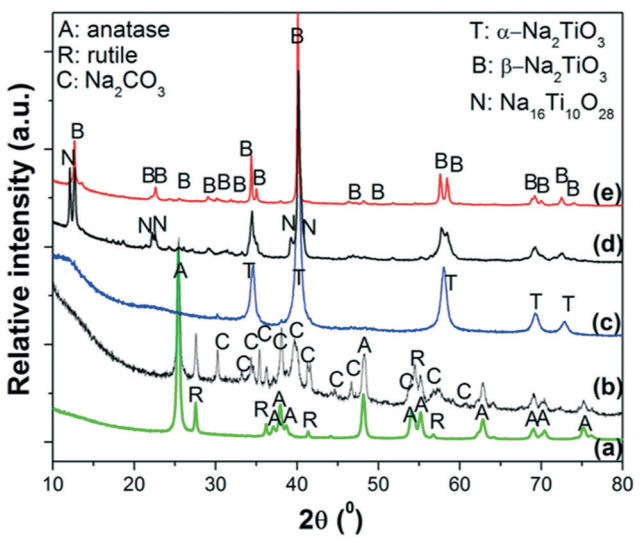

Fig. 3 XRPD patterns of: a) starting powders of nano-TiO_2; b) as-milled 2NaOH–TiO_2 mixture; heating up to c) 650 °C, d) 800 °C and e) 800 °C, 5 h. Heating ramp: 5 °C min^{-1} in synthetic air.

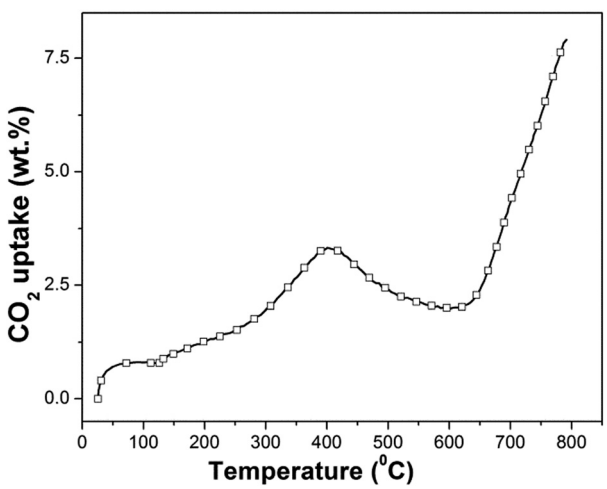

Fig. 4 Dynamic thermogravimetric analysis of synthesized β-Na_2TiO_3. Heating ramp: 5 °C min^{-1}; 50 cm^3 min^{-1} STP of CO_2.

The dynamic thermogram showing a weight increment followed by a weight decrement, and a subsequent weight increment, is not in line with previous results reported for other CO_2 sorbents, which typically exhibit two consecutive weight increments as a function of increasing temperature (the first one is associated with CO_2 chemisorption and the second one is associated with CO_2 absorption). However, our results show similarities to the only non-isothermal previous study on Na_2TiO_3,[27] although there are differences in the temperature ranges where the CO_2 capture and weight loss were observed. In the above-mentioned report, the authors attribute the abnormal dynamic thermogram of Na_2TiO_3 to a different temperature-dependent CO_2 capture reaction mechanism, and to the poor thermal stability of the ceramic.

3.2 *In situ* synchrotron X-ray diffraction analysis

Three *in situ* XRD experiments were carried out with the aim of understanding: 1) the reaction mechanism of Na_2TiO_3 during high temperature carbonation, and 2) the effect of the initial atmosphere on the reaction path and kinetics.

The experiments involved dynamic heating under either a N_2 or CO_2 flow followed by isothermal conditions at selected temperatures under a CO_2 gas flow. The proposed measurements allowed distinguishing structural changes derived from the reaction of Na_2TiO_3 with CO_2 from thermally driven changes that may occur due to the instability of the material. Furthermore, the preheating of the samples under a N_2 flow allowed mimicking the procedure commonly used to characterize carbonation reaction products by *ex situ* methods. In this procedure, samples are first heated to a selected temperature under an inert gas atmosphere and then exposed to CO_2 for 1 or 2 hours. Therefore, the obtained results also will serve to visualize the limitations that these procedures might present for obtaining an accurate description of high temperature carbonation reactions. This is essential to relate chemical processes to dynamic TG CO_2 sorption curves.

3.2.1 Na_2TiO_3 heated under N_2 followed by isothermal heating at 615 °C under CO_2. Na_2TiO_3 was subjected to continuous heating at a ramp of 5 °C min^{-1} under an inert gas flow up to 615 °C. Once this temperature was reached, the gas was switched to CO_2 and the sample was kept under isothermal conditions for 1 h. Fig. 5a displays the evolution of the X-ray diffraction patterns upon heating, and Fig. 5b shows the corresponding phase composition and temperature evolution. Interestingly, it is possible to notice that at 40 °C (initial temperature of the experiment), β-Na_2TiO_3 already has suffered a partial transition and the resulting material is a mixture of β-Na_2TiO_3, a secondary phase and a very small fraction of Na_2CO_3 that could be formed due to CO_2 chemisorption derived from air exposure. It is important to remark that the initial composition of the system is different from the one observed right after the synthesis process. The secondary phase was indexed using DICVOL06 (ref. 35) and the results showed good agreement with a monoclinic lattice having the following parameters: a = 6.6651 Å, b = 4.6488 Å, c = 3.4209 Å and β = 110.1°. This phase is indicated within the figures as m-Na_2TiO_3, and to the best of our knowledge, it has not been previously reported. The presence of the β-Na_2TiO_3 phase accompanying the monoclinic one hinders any attempt to determine other structural parameters of this phase, such as atomic positions. The monoclinic phase reverts to β-Na_2TiO_3 after reaching 300 °C, as can be seen in the patterns presented in Fig. 5a, where the characteristic reflections of the monoclinic phase, such as the peak at 2θ = 5.22°, disappear. Simultaneously, the small percentage of Na_2CO_3 also decreases, indicating the release of CO_2. This is accompanied by the subtle appearance of reflections corresponding to the Na_2O phase. According to

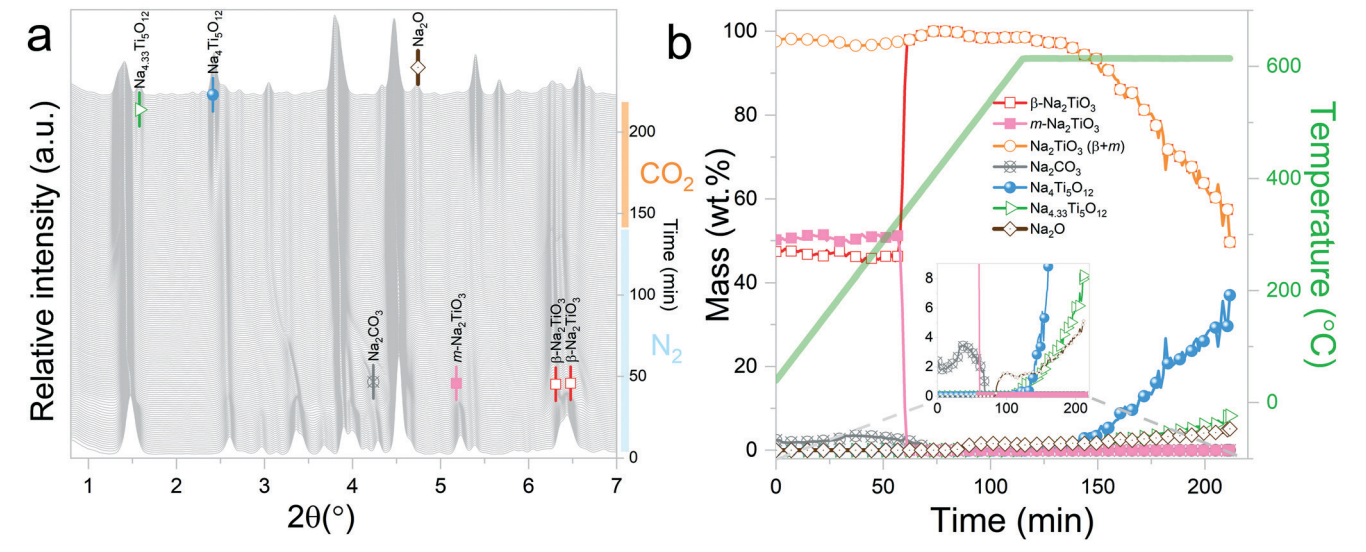

Fig. 5 Na_2TiO_3 heating under a N_2 flow until 615 °C, followed by isothermal conditions under a CO_2 gas flow: a) evolution of X-ray diffraction patterns upon heating; b) phase evolution (wt%) as a function of time and temperature.

Sánchez-Camacho *et al.*,[27] these results can be explained by CO_2 chemisorption followed by CO_2 release, caused by the heating, which would lead to the formation of an external shell of Na_2O. From the figure, it can be noticed that β-Na_2TiO_3 remains stable up to 600 °C under an inert atmosphere. Once the gas flow is switched to CO_2, β-Na_2TiO_3 undergoes partial decomposition into $Na_{4.33}Ti_5O_{12}$ (01-084-8819 PDF file) and $Na_4Ti_5O_{12}$ (00-052-1814 PDF file). The disproportionation follows reactions (4) and (5), respectively.

$$5Na_2TiO_3 \rightarrow Na_{4.33}Ti_5O_{12} + 2.835Na_2O + 0.0825O_2 \quad (4)$$

$$5Na_2TiO_3 \rightarrow Na_4Ti_5O_{12} + 3Na_2O \quad (5)$$

Sánchez-Camacho *et al.*[27] propose reaction (6) as an intermediary step for reaction (5), suggesting that Na_2CO_3 is not observed because it immediately decomposes following reaction (7).

$$5Na_2TiO_3 + 3CO_2 \rightarrow 3Na_2CO_3 + Na_4Ti_5O_{12} \quad (6)$$

$$Na_2CO_3 \rightarrow CO_2 + Na_2O_{(sub)} \quad (7)$$

3.2.2 Na_2TiO_3 heated under N_2 followed by isothermal heating at 770 °C under CO_2. Na_2TiO_3 was heated to 770 °C at a ramp of 5 °C min^{-1} under an inert gas flow. At 770 °C, the gas was switched to CO_2 and the sample was kept under isothermal conditions for 1 h. The initial diffractograms for this measurement (Fig. 6a) display a similar phase mixture to the previous one (Fig. 6b) with a difference in composition of 2%, which is well within the margin of error. As expected, the sample follows the same path as the previous one until around 630 °C. At this temperature, β-Na_2TiO_3 decomposes showing the appearance of a new phase, which is similar to the $Na_{16}Ti_{10}O_{28}$ structure previously reported by Mayer and Perez[36] (01-076-0686 PDF file). This phase was also observed by Sánchez-Camacho *et al.*[27] However, the intensity ratios between some reflections do not match the expected values. This could be an indication of an isostructural phase with a slightly different composition. Unfortunately, the presence of secondary phases makes it difficult to determine the exact difference in the stoichiometry. A proposed reaction mechanism is presented in eqn (8).

$$10Na_2TiO_3 \rightarrow Na_{16}Ti_{10}O_{28} + 2Na_2O \quad (8)$$

Interestingly, it should be noticed that in the previously mentioned work, the proposed reaction pathway considers β-Na_2TiO_3 carbonation as an intermediary step for reaction (8). However, our results show that reaction (8) occurs even in the absence of CO_2. The results from these measurements also confirm the proposition of Sánchez-Camacho[27] regarding eqn (6) being a required intermediary step for reaction (5), since this decomposition to $Na_4Ti_5O_{12}$ is not observed under a N_2 flow. Peaks belonging to Na_2O can also be observed up to 770 °C, the temperature at which the sample atmosphere is changed to CO_2. At this stage, new reflections emerge, indicating the formation of an additional phase. The new peaks were indexed to the $Na_{0.97}Ti_2O_4$ phase (04-014-7035 PDF file). Since this transition only occurs in the presence of a CO_2 gas flow, it is possible to assume that Na_2CO_3 plays a role as an intermediate product of this decomposition. A possible reaction path is presented in eqn (9).

$$2Na_{16}Ti_{10}O_{28} + 11.15CO_2 \rightarrow 10Na_{0.97}Ti_2O_4 + 11.15Na_2CO_3 + 2.425O_2 \quad (9)$$

3.2.3 Na_2TiO_3 heated under CO_2 followed by isothermal heating at 770 °C. β-Na_2TiO_3 was heated at a ramp of 5 °C min^{-1} under a CO_2 gas flow, until reaching a temperature of 770 °C. Once this temperature was reached, the sample was

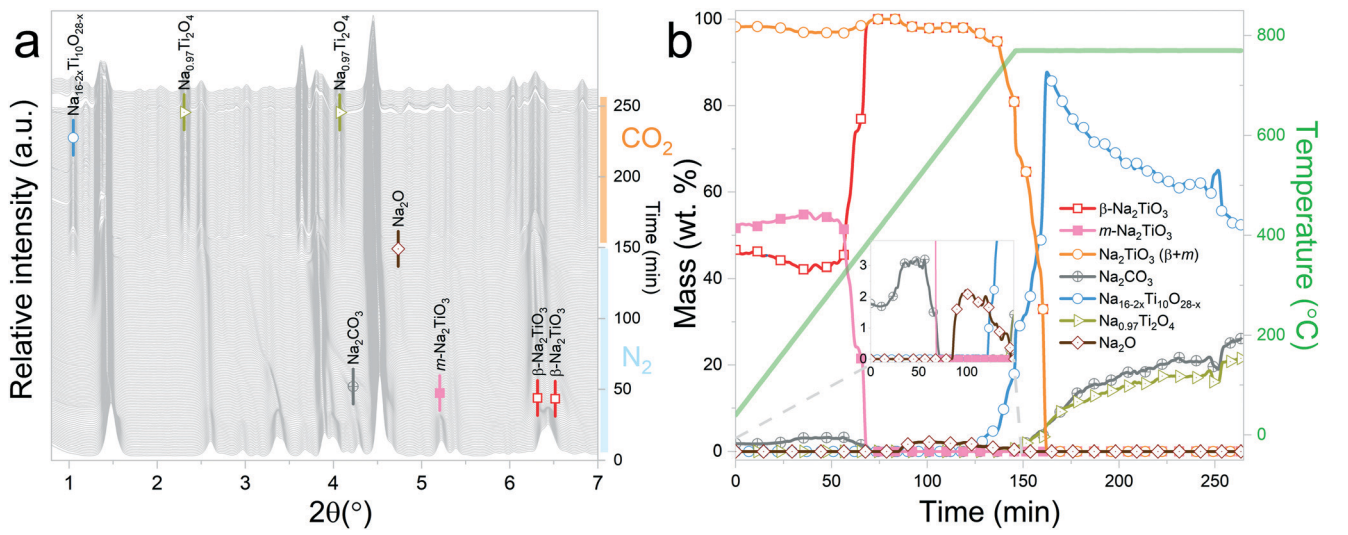

Fig. 6 Na_2TiO_3 heating under a N_2 flow until 770 °C, followed by isothermal conditions under a CO_2 gas flow: a) evolution of X-ray diffraction patterns upon heating; b) phase evolution (wt%) as a function of time and temperature.

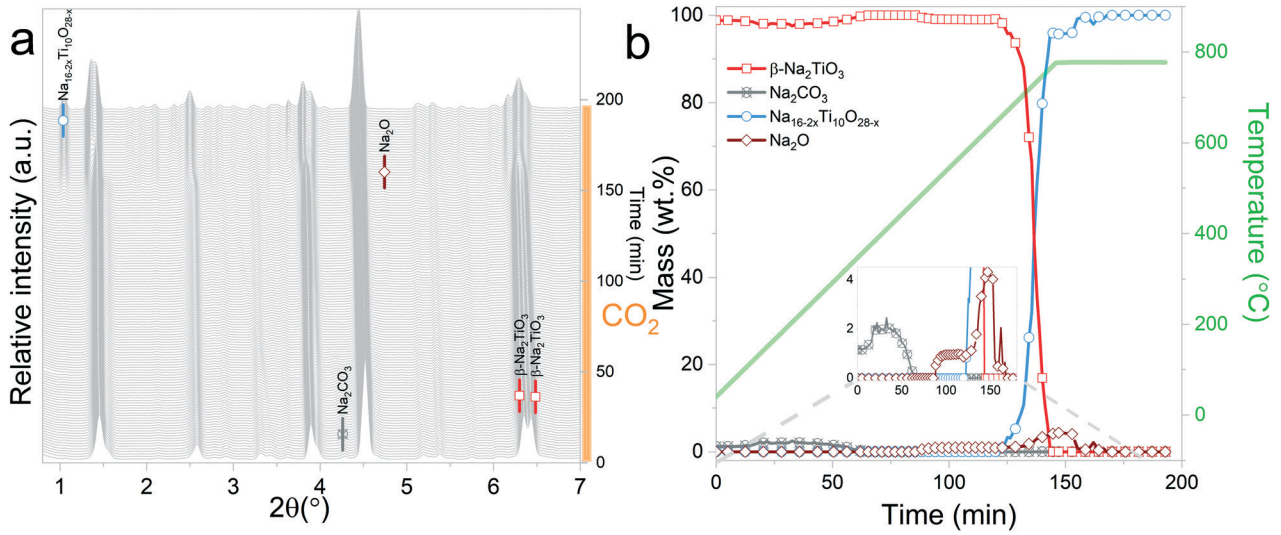

Fig. 7 Na_2TiO_3 heating under a CO_2 gas flow, followed by isothermal conditions at 770 °C: a) evolution of X-ray diffraction patterns during heating; b) phase evolution (wt%) as a function of time and temperature.

kept under isothermal conditions. As it can be observed from Fig. 7a and b, the phase composition of the starting material differs from the ones observed in the previous measurements, in which the heating process was performed under an inert gas flow. In this case, the sample exhibits almost pure β-Na_2TiO_3. Although the reason for this is not clear, it could be speculated that the presence of CO_2 inhibits the growth of the monoclinic phase.

At the initial stages of heating, the XRD patterns display an almost negligible amount of Na_2CO_3, which is evidenced by the presence of the two main peaks corresponding to this phase at 2θ = 3.989° (overlapping with a secondary peak of Na_2TiO_3) and 2θ = 4.289°. During the first stage of the heating process, a slight increment in the amount of carbonate can be observed, but after reaching 300 °C, it starts to diminish. At 350 °C, no trace of Na_2CO_3 can be detected. Between 350 °C and 660 °C, β-Na_2TiO_3 is the only phase remaining. This is consistent with the TG results shown in Fig. 4, and also with previously reported curves,[27] in which the absorption of CO_2 into similar samples is only observed at temperatures starting from 675 °C. At this temperature, a phase change occurs, evidenced by the subtle appearance of new peaks. Some of these new peaks match the ones observed in the previous measurement, indicating the presence of a $Na_{16}Ti_{10}O_{28}$-like structure. In this case, due to the higher abundance of this phase, it was possible to perform a deeper analysis of the XRD data. A refinement of the final diffractogram (Fig. 8) showed a higher number of sodium and oxygen vacancies compared to the one observed by Sánchez-Camacho *et al.*,[27] indicating a composition more in line with a $Na_{16-2x}Ti_{10}O_{28-x}$ formula, with x in the range 0.1–0.25. This leads to a slightly modified eqn (8) as follows:

$$10Na_2TiO_3 \rightarrow Na_{16-2x}Ti_{10}O_{28-x} + (2 + x)Na_2O \quad (10)$$

By observing Fig. 7, it is clear that a second reaction resulting in the formation of $Na_{0.97}Ti_2O_4$ does not occur. This is difficult to understand since at this stage, the temperature and gas flow conditions are comparable to those in the previous experiment. A possible explanation is that the CO_2 gas flow generates a change in the morphology of Na_2TiO_3 by preventing the first transition towards the monoclinic phase. These changes then are transferred to $Na_{16-2x}Ti_{10}O_{28-x}$, inhibiting the further decomposition of the titanate. As it can be observed from Fig. 5, reaction (9) is very slow, so it may be possible that an unfavorable particle morphology, such as larger crystallite sizes[33] or larger diffusion paths, could make this reaction impossible to see in the time frame of the experiment. A closer inspection toward the last XRD pattern

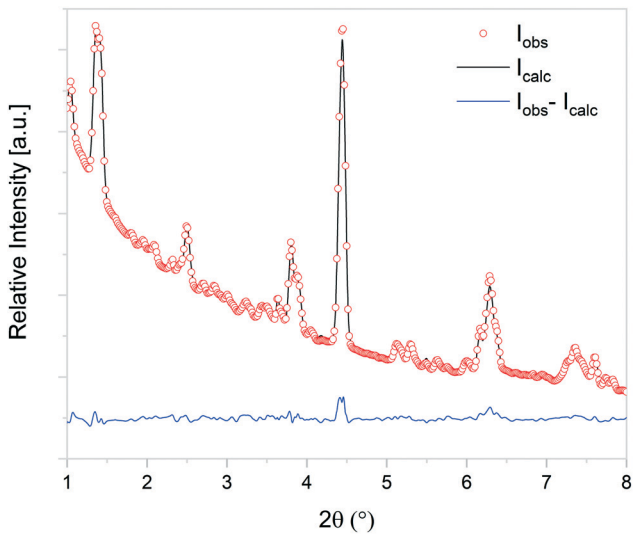

Fig. 8 Observed (open circles) and calculated (line) X-ray diffraction patterns of $Na_{16-2x}Ti_{10}O_{28-x}$, with x in the range 0.1–0.25.

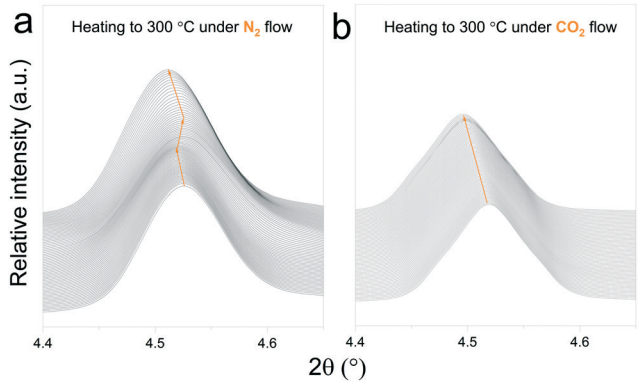

Fig. 9 Structural changes of Na_2TiO_3 under dynamic heating at a ramp of 5 °C min^{-1} under a N_2 flow (a) and CO_2 flow (b).

from these measurements showed a faint hint of the characteristic peak of $Na_{0.97}Ti_2O_4$ at $2\theta = 1.9°$. This different morphology could also be an explanation about why the decomposition into $Na_4Ti_5O_{12}$ and $Na_{4.33}Ti_5O_{12}$ is not observed here, since those two reactions are much slower than the decomposition to $Na_{16-2x}Ti_{10}O_{28-x}$, as can be seen by comparing Fig. 5b and 6b.

3.3 Effect of the initial atmosphere on the Na_2TiO_3–CO_2 reaction pathway

In situ X-ray diffraction analysis for real-time monitoring of chemical reactions on CO_2 capture materials[15,37–40] has been proven to be a useful tool to understand the behaviour of CO_2 sorbents at temperatures that are relevant for real applications, allowing the identification of structural changes, to reveal intermediate phases and re-conversion processes occurring during operational conditions[29,41] and to investigate the impact of the presence of H_2O in the gas stream.[42] However, due to the limited access to powerful X-ray probes, many reports have proposed carbonation mechanisms of these materials based on *ex situ* X-ray diffraction data.[27,43] Typically, *ex situ* samples are obtained after heating different samples under an inert atmosphere, switching the gas flow to CO_2 once the desired temperature is reached and then maintaining isothermal conditions for a couple of hours. The results obtained by these procedures can provide valuable insights into the reaction mechanism of CO_2 sorbents. However, the results presented in this work indicate that thermal preheating under an inert atmosphere can severely affect the structure of the sorbent prior to its exposure to CO_2. In Fig. 9ab and , a selected 2θ region in which Na_2TiO_3 is heated under a N_2 and CO_2 gas flow, respectively, is displayed. From Fig. 9a, it can be observed that there is a transition from monoclinic Na_2TiO_3 to β-Na_2TiO_3 when the sample is subjected to a N_2 flow. As shown in the previous subsection, these structural changes can influence the further dynamic evolution of the material by either slowing or speeding up the next reaction steps. Although these transitions are difficult to observe with traditional methods, they are critical to explain the dynamic CO_2 capture thermograms. This further emphasizes the need for *in situ* tools to obtain an accurate description of the CO_2 capture performance of sorbent materials.

4 Conclusions

Na_2TiO_3 was successfully synthesized from NaOH and TiO_2 *via* a solid state route, where the powder mixture was heat treated at 800 °C for 5 h. The CO_2 sorption properties of synthesized Na_2TiO_3 were analyzed by dynamic thermogravimetric analysis.

In situ synchrotron XRD analysis, performed to study the reaction mechanism of Na_2TiO_3 at high temperatures in the presence of CO_2, revealed the complex behaviour of the Na–Ti–O system. With the aim of differentiating phase transformations driven by carbonation processes from those occurring as a consequence of the thermal stability of the ceramic, the high temperature behavior of Na_2TiO_3 under different gas flows was studied. A careful analysis of Na_2TiO_3 phase transitions showed that its structure can be strongly influenced by the surrounding atmosphere.

At 40 °C, samples subjected to a N_2 flow show the presence of β-Na_2TiO_3 and monoclinic Na_2TiO_3 phases, while the sample subjected to a CO_2 flow showed no evidence of the latter. This difference in composition disappears upon heating, when the monoclinic phase reverts to β-Na_2TiO_3. Further heating at temperatures above 650 °C causes β-Na_2TiO_3 to transition to $Na_{16-2x}Ti_{10}O_{28-x}$. This transition occurs under either a pure N_2 or CO_2 gas flow. However, at this point, while the samples have reached a similar situation in terms of phase composition and environmental conditions, the previous history of the sample seems to play a role in the kinetic behaviour of the system. In both cases, when subjected to a CO_2 flow, $Na_{16-2x}Ti_{10}O_{28-x}$ undergoes a carbonation process. However, although both samples showed similar reaction paths, considerable differences in the reaction kinetics between both have been observed. The retardation effect observed for the sample preheated under CO_2 is evident in the results, and it can be attributed to morphological differences related to the lack of transition from the monoclinic phase, which could influence the diffusion processes required for the carbonation of $Na_{16-2x}Ti_{10}O_{28-x}$.

The differences found when subjecting Na_2TiO_3 to different atmospheres upon heating demonstrate that *in situ* XRD characterization is essential to monitor in real time the structural changes that occur to the system and to correlate them to dynamic TG observations, providing a much reliable insight on the chemical processes that take place during sorption reactions.

Conflicts of interest

"There are no conflicts to declare".

Acknowledgements

The authors thank the European Synchrotron Radiation Facility for in-house beamtime allocation and financial support, and Florian Rusello and Tiago Coutinho for their help with the preparation of the experimental setup. This work was partially supported by CONICET, ANPCyT – (PICT 2018-00606), CNEA and Cuyo University.

Notes and references

1 O. US EPA, *Global Non-CO2 GHG Emissions: 1990–2030*, 2016, https://www.epa.gov/global-mitigation-non-co2-greenhouse-gases/global-non-co2-ghg-emissions-1990-2030.
2 A. Alonso, J. Moral-Vico, A. Abo Markeb, M. Busquets-Fité, D. Komilis, V. Puntes, A. Sánchez and X. Font, *Sci. Total Environ.*, 2017, **595**, 51–62.
3 Q. Wang, J. Luo, Z. Zhong and A. Borgna, *Energy Environ. Sci.*, 2011, **4**, 42–55.
4 A. Samanta, A. Zhao, G. K. H. Shimizu, P. Sarkar and R. Gupta, *Ind. Eng. Chem. Res.*, 2012, **51**, 1438–1463.
5 J. Wang, L. Huang, R. Yang, Z. Zhang, J. Wu, Y. Gao, Q. Wang, D. O'Hare and Z. Zhong, *Energy Environ. Sci.*, 2014, **7**, 3478–3518.
6 M. G. Plaza, S. Martínez and F. Rubiera, *Energies*, 2020, **13**, 5692.
7 T. O. Nelson, A. Kataria, P. Mobley, M. Soukri and J. Tanthana, *Energy Procedia*, 2017, **114**, 2506–2524.
8 E. R. van Selow, P. D. Cobden, P. A. Verbraeken, J. R. Hufton and R. W. van den Brink, *Ind. Eng. Chem. Res.*, 2009, **48**, 4184–4193.
9 P. Pecharaumporn, S. Wongsakulphasatch, T. Glinrun, A. Maneedaeng, Z. Hassan and S. Assabumrungrat, *Int. J. Hydrogen Energy*, 2019, **44**, 20663–20677.
10 B. Dou, C. Wang, Y. Song, H. Chen, B. Jiang, M. Yang and Y. Xu, *Renewable Sustainable Energy Rev.*, 2016, **53**, 536–546.
11 C. S. Martavaltzi, E. P. Pampaka, E. S. Korkakaki and A. A. Lemonidou, *Energy Fuels*, 2010, **24**, 2589–2595.
12 D. M. D'Alessandro, B. Smit and J. R. Long, *Angew. Chem., Int. Ed.*, 2010, **49**, 6058–6082.
13 Y. Zhang, Y. Gao, H. Pfeiffer, B. Louis, L. Sun, D. O'Hare and Q. Wang, *J. Mater. Chem. A*, 2019, **7**, 7962–8005.
14 Y. Hu, W. Liu, Y. Yang, M. Qu and H. Li, *Chem. Eng. J.*, 2019, **359**, 604–625.
15 M. L. Grasso, M. V. Blanco, F. Cova, J. A. González, P. A. Larochette and F. C. Gennari, *Phys. Chem. Chem. Phys.*, 2018, **20**, 26570–26579.
16 C. Wang, B. Dou, Y. Song, H. Chen, Y. Xu and B. Xie, *Ind. Eng. Chem. Res.*, 2014, **53**, 12744–12752.
17 T. Ávalos Rendón, J. Casa-Madrid and H. Pfeiffer, *J. Phys. Chem. A*, 2009, **113**, 6919–6923.
18 Q. Zheng, L. Huang, Z. Zhong, B. Louis and Q. Wang, *Chem. Eng. J.*, 2020, **380**, 122444.
19 G. Ji, M. Z. Memon, H. Zhuo and M. Zhao, *Chem. Eng. J.*, 2017, **313**, 646–654.
20 R. Rodríguez-Mosqueda and H. Pfeiffer, *J. Phys. Chem. C*, 2013, **117**, 13452–13461.
21 J. Liu, Z. Wang, Z. Wang, J. Song, G. Li, Q. Xu, J. You, H. Cheng and X. Lu, *Phys. Chem. Chem. Phys.*, 2019, **21**, 13135–13143.
22 A. López-Ortiz, N. G. P. Rivera, A. R. Rojas and D. L. Gutierrez, *Sep. Sci. Technol.*, 2005, **39**, 3559–3572.
23 G. Ji, H. Yang, M. Z. Memon, Y. Gao, B. Qu, W. Fu, G. Olguin, M. Zhao and A. Li, *Appl. Energy*, 2020, **267**, 114874.
24 S. Song, M. Kotobuki, Y. Chen, S. Manzhos, C. Xu, N. Hu and L. Lu, *Sci. Rep.*, 2017, **7**, 373.
25 T. Kobayashi, W. Zhao, H. B. Rajendra, K. Yamanaka, T. Ohta and N. Yabuuchi, *Small*, 2020, **16**, 1902462.
26 Q. Liu, Z. Hu, W. Li, C. Zou, H. Jin, S. Wang, S. Chou and S.-X. Dou, *Energy Environ. Sci.*, 2021, **14**, 158–179.
27 P. Sánchez-Camacho, I. C. Romero-Ibarra, Y. Duan and H. Pfeiffer, *J. Phys. Chem. C*, 2014, **118**, 19822–19832.
28 H. Outokumpu, *HSC Chemistry For Windows Version 6.1*, 2009.
29 F. Cova, G. Amica, K. Kohopää and M. V. Blanco, *Inorg. Chem.*, 2019, **58**, 1040–1047.
30 J. Kieffer and D. Karkoulis, *J. Phys.: Conf. Ser.*, 2013, **425**, 202012.
31 M. Wojdyr, *J. Appl. Crystallogr.*, 2010, **43**, 1126–1128.
32 B. H. Toby and R. B. Von Dreele, *J. Appl. Crystallogr.*, 2013, **46**, 544–549.
33 F. Meng, Y. Liu, T. Xue, Q. Su, W. Wang and T. Qi, *RSC Adv.*, 2016, **6**, 112625–112633.
34 M. L. Grasso, P. Arneodo Larochette and F. C. Gennari, *J. CO2 Util.*, 2020, **38**, 232–240.
35 A. Boultif and D. Louër, *J. Appl. Crystallogr.*, 2004, **37**, 724–731.
36 M. Mayer and G. Perez, *Rev. Chim. Miner.*, 1976, **13**, 237–242.
37 R. Molinder, T. P. Comyn, N. Hondow, J. E. Parker and V. Dupont, *Energy Environ. Sci.*, 2012, **5**, 8958–8969.
38 M. T. Dunstan, S. A. Maugeri, W. Liu, M. G. Tucker, O. O. Taiwo, B. Gonzalez, P. K. Allan, M. W. Gaultois, P. R. Shearing, D. A. Keen, A. E. Phillips, M. T. Dove, S. A. Scott, J. S. Dennis and C. P. Grey, *Faraday Discuss.*, 2016, **192**, 217–240.
39 A. Biasin, C. U. Segre and M. Strumendo, *Cryst. Growth Des.*, 2015, **15**, 5188–5201.
40 J. Manuel Valverde, A. Perejon, S. Medina and L. A. Perez-Maqueda, *Phys. Chem. Chem. Phys.*, 2015, **17**, 30162–30176.
41 M. V. Blanco, K. Kohopää, I. Snigireva and F. Cova, *Chem. Eng. J.*, 2018, **354**, 370–377.
42 J. M. Valverde and S. Medina, *Phys. Chem. Chem. Phys.*, 2017, **19**, 7587–7596.
43 F. Durán-Muñoz, I. C. Romero-Ibarra and H. Pfeiffer, *J. Mater. Chem. A*, 2013, **1**, 3919–3925.